# Appearance of cluster states in $^{13}$C

T. Yoshida,[1] N. Itagaki,[2] and T. Otsuka[2,3]

[1]*Meme Media Laboratory, Hokkaido University, Sapporo 060-8628, Japan*
[2]*Department of Physics, University of Tokyo, Hongo, Tokyo 113-0033, Japan*
[3]*Center for Nuclear Study, University of Tokyo, Hongo, Tokyo 113-0033, Japan*

We study the structure of low-lying states of $^{13}$C with a microscopic cluster model. In addition to the $3\alpha$-$n$ model space, the breaking effect of one of the $\alpha$ clusters due to the spin-orbit interaction is also taken into account. The isoscalar $E0$ transition probabilities from the ground $1/2^-$ state to the excited ones are discussed associated with the cluster structure of these states.

## I. INTRODUCTION

Various microscopic cluster models have been successfully applied to light nuclei [1,2], and recently, the analysis has been extended to the neutron-rich side. For instance, Be isotopes have been analyzed to have an $\alpha + \alpha$ cluster structure with the valence neutrons [3–10]. We have discussed that the anomalously large cluster structure of $\alpha + \alpha$, which appears in $^{10}$Be and $^{12}$Be, is associated with the $\sigma$ orbital of the valence neutrons.

As the next step of such studies, we focus on the $3\alpha$-cluster structure of C isotopes. The second $0^+$ state of $^{12}$C has been well known to have a developed $3\alpha$-cluster structure (Hoyle state), which has been recently reinterpreted as an $\alpha$-condensed state [11,12]. It is intriguing to see how the structure changes when valence neutrons are added in neutron-rich C isotopes. Because the attractive interaction acts between the neutrons and the $3\alpha$ core, the gas-like cluster structure of the second $0^+$ state of $^{12}$C is changed to a state with a geometric shape. For instance, an equilateral-triangular shape of $3\alpha$, which is stabilized by the additional two valence neutrons, is suggested in $^{14}$C based on the molecular-orbit model [13]. When the system has this symmetry, a rotational band structure with $K^\pi = 3^-$ appears in addition to that with $K^\pi = 0^+$ [2,14]. Experimentally, the candidates for these bands have been observed and the members of these bands are well excited by $\alpha$-transfer reactions, which strongly suggests the $\alpha$-cluster structure [15].

In this article, we study $^{13}$C, which is the nucleus located between $^{12}$C and $^{14}$C on the nuclear chart, and we study how the gas-like cluster state of $^{12}$C changes when one valence neutron is added. Recently, the presence of the cluster states in $^{13}$C has been suggested by measuring the isoscalar $E0$ transitions from the ground $1/2^-$ state induced by the $^{13}$C$(\alpha, \alpha')^{13}$C reaction [16]. The obtained values are much larger than those of the shell-model calculations, which suggests that protons and neutrons are coherently excited and they have spatially extended distribution in the excited states. However, the values are smaller if we compare them with the $B(E0)$ value of $^{12}$C from the ground $0^+$ state to the $0_2^+$ state. Analysis from the theoretical side is required to see whether or not this implies a structure change of the Hoyle state due to the additional neutron. Also, other candidates for the $\alpha$-cluster states are

suggested around the $E_x = 10$ MeV region. Here, in addition to a linear-chain configuration of $3\alpha$ clusters [17], the presence of the states with the two-dimensional $3\alpha$ configurations is suggested [17–19].

Recently, the cluster states of $^{13}$C and their relation to the $E0$ transition have been discussed based on the orthogonal condition model (OCM) [20]. Here, the model space is $3\alpha + n$ (four-body). We introduce a microscopic model, in which an $\alpha$-breaking effect due to the coupling with the shell-model-like configurations is also included. The breaking effect of one of the $\alpha$ clusters due to the spin-orbit interaction is expressed by introducing the simplified method to include the spin-orbit interaction (SMSO) [21,22].

This article is organized as follows: in Sec. II, the framework is described, and in Sec. III, numerical results are presented. In Sec. IV, possible interpretations of the obtained results, especially for the $B(E0)$ values, are discussed, and the conclusion is given in Sec. V.

## II. FRAMEWORK

The total wave function is fully antisymmetrized and is given by a superposition of the Slater determinants ($\{\Psi_k\}$) with coefficients $\{c_k\}$:

$$\Phi = \sum_k c_k P_{MK}^J \Psi_k. \tag{1}$$

Projection onto a good angular momentum is performed by the projection operator $P_{MK}^J$, and the coefficients $\{c_k\}$ are determined by diagonalizing the Hamiltonian matrix after this projection. Each Slater determinant ($\Psi_k$) consists of $A$ nucleons

$$\Psi_k = \mathcal{A}[(\psi_1 \chi_1)(\psi_2 \chi_2) \cdots]. \tag{2}$$

and each nucleon ($\psi_i \chi_i$, $i = 1 \sim A$) has a Gaussian form the same as many conventional cluster models. The oscillator parameter ($b = 1/\sqrt{2\nu} = 1.46$ fm) is common for all nucleons to exactly remove the center-of-mass kinetic energy. Each $\alpha$ cluster is expressed by giving a common $\vec{z}_i$ value for four nucleons (proton spin-up, proton spin-down, neutron spin-up, and neutron spin-down).

We introduce two kinds of model spaces. One is the cluster model space $\Psi_{cl}$ with various $3\alpha + n$ configurations, and the other is model space $\Psi_{ab}$, in which the breaking effect of one of the $\alpha$ clusters is taken into account. In both model spaces, the position of the Gaussian center parameter for one valence neutron is randomly generated. In $\Psi_{ab}$, the inclusion of the breaking effect of one of the $\alpha$ clusters is achieved by employing the simplified method to include the spin-orbit contribution (SMSO) [21,22]. In the SMSO, we introduce the imaginary part for the Gaussian center parameters of one of the $\alpha$ clusters to be broken, which enables us to take into account the contribution of the spin-orbit interaction for this cluster. The four nucleons in the $\alpha$ clusters to be broken have a common spatial part of $\phi_{\vec{Z}}$ centered at $\vec{R}$,

$$\phi_{\vec{Z}} = \exp\{-\nu(r - \vec{Z}/\sqrt{\nu})^2\} \tag{3}$$

$$\text{Re}[\vec{Z}/\sqrt{\nu}] = \vec{R}. \tag{4}$$

When the $\alpha$ breaking due to the spin-orbit interaction is considered, in addition to the real part of $\vec{Z}$, the imaginary part is introduced dependent of the spin orientation of each nucleon in this $\alpha$ cluster ($\vec{e}_s$ is the unit vector for the spin orientation of the nucleon):

$$\text{Im}[\vec{Z}/\sqrt{\nu}] = \Lambda(\vec{e}_s \times \vec{R}). \tag{5}$$

The introduction of the imaginary part of $\vec{Z}$ enables us to consider the spin-orbit contribution, and $\Lambda$ is the order parameter of the transition from a pure $\alpha$-cluster configuration to a $jj$-coupling-like configuration as discussed in Refs. [21–23].

For the Hamiltonian, we use the Volkov No. 2 ($V2$) potential [24] for the central part and the G3RS potential [25] for the spin-orbit part as the effective $N$-$N$ interactions. To reproduce the scattering phase shifts of the $\alpha + n$ and $\alpha + \alpha$ systems, $M$ (Majorana parameter of $V2$) $= 0.6$ and $V_0$ (strength of G3RS) $= 2000$ MeV should be adopted [26]. However, for the carbon isotopes, these parameters are found to lead systematic overbinding [27]. One origin must be the missing of the tensor interaction, whose first order contribution (between $j$-upper protons and $j$-upper neutrons [28]) acts repulsively when an $\alpha$ cluster is broken to take into account the spin-orbit interaction. To include this effect in the present Hamiltonian, $V_0$ is slightly modified to 1500 MeV. Also, we introduce the Bartlet and Heisenberg terms as $B = H = 0.125$ to reproduce the binding energy of deuteron and to remove the bound state of the neutron-neutron system. In addition, we compare the results calculated with the Majorana exchange parameters of $M = 0.6$ and 0.61.

## III. RESULTS

First, we show how the energy eigen states are obtained. The energy convergence of the $1/2^-$ states calculated within the bound state approximation is shown in Fig. 1 ($M = 0.61$ case), where the horizontal axis is the number of basis states. The basis states of $\Psi_{cl}$ are from 1 to 250 with the $3\alpha + n$ model space, and the basis states of $\Psi_{ab}$ are from 251 to 400, where the $\alpha$-breaking effect is taken into account using SMSO. The $\Lambda$ value of each basis state in $\Psi_{ab}$ is determined by optimizing the energy of the negative parity state of each basis

state; however, the basis states with $\Lambda < 0.2$ are excluded. In addition, we include the basis states whose $\Lambda$ values are artificially doubled from those obtained above. As for the selection of the basis states, we use the idea of the stochastic variational method (SVM) [29]. When $N$ basis states are selected, the $(N + 1)$-th Slater determinant is adopted under the condition of $\sum_i |E_{i,N+1} - E_{i,N}| < 0.1$ MeV, where the summation over $i$ is for the six lowest $1/2^-$ states. This is needed to obtain the basis states not only for the ground state, but also for the excited states. Also, if the eigenvalue of the norm matrix becomes $10^{-12}$ times smaller compared to the largest one, then we exclude such states for numerical stability. As a result, 97 $\Psi_{cl}$ states are selected out of 250, and 32 $\Psi_{ab}$ states are selected out of 150. The curves show that after getting convergence within $\Psi_{cl}$, energies decrease again when we start incorporating the model space of $\Psi_{ab}$. The decrease of the energy due to the mixing of $\Psi_{ab}$ is large ($\sim 5$ MeV) for the first and the second $1/2^-$ states. Here, the lowest $1/2^-$ state at $-94.3$ MeV corresponds to the ground state, which is bound by 11.6 MeV from the $\alpha$-$\alpha$-$\alpha$-$n$ threshold ($-82.7$ MeV) in good agreement with the experimental value of 12.2 MeV. The second $1/2^-$ state, which converges at $-81.3$ MeV, is the fourth state within $\Psi_{cl}$ before introducing the $\alpha$-breaking configurations ($\Psi_{ab}$), and the coupling effect between the two configurations is really large for this state. Contrary to the two lowest $1/2^-$ states, the third and fourth $1/2^-$ states do not show large energy decrease due to the mixing of $\alpha$-breaking configurations. This might indicate the persistence of an $\alpha$-cluster structure in these states.

For $\Psi_{ab}$, we have introduced the $\Lambda$ parameter as an order parameter of the $\alpha$-breaking states; however, because we have superposed states with different $\Lambda$ values and $\Lambda$ is not observable, we must introduce a different quantity in operator form to extract the amount of the mixing of $\alpha$-breaking components. Here, a one-body $ls$ operator (SO$_{1by}$) is introduced for the proton part:

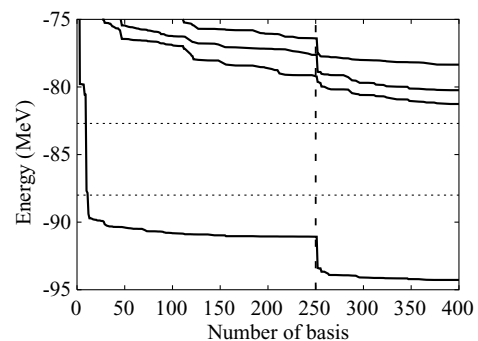$$\text{SO}_{1by} = \sum_{i=\text{protons}} \vec{L}_i \cdot \vec{S}_i. \tag{6}$$



FIG. 1. The energy convergence for the $J^\pi = 1/2^-$ states of $^{13}$C within the bound state approximation. The horizontal axis shows the number of trial Slater determinants. The basis states of the $3\alpha + n$ model space ($\Psi_{cl}$) are from 1 to 250, and the $\alpha$-breaking effect is taken into account in 251–400. The dashed lines at $-88.0$ MeV and $-82.7$ MeV show the $^{12}$C$+n$ and $\alpha$-$\alpha$-$\alpha$-$n$ threshold energy, respectively. The Majorana parameter of $V2$ is taken to be $M = 0.61$.

TABLE I. The calculated properties of each $1/2^-$ state of $^{13}$C within the bound state approximation. The energy ($E$), the expectation values of a one-body spin-orbit operator ($SO_{1by}$), the proton and matter rms radii (fm), and the single-particle parity of a valence neutron ($P_v$) are shown.

|  | $1/2_1^-$ | $1/2_2^-$ | $1/2_3^-$ | $1/2_4^-$ | $1/2_5^-$ |
|---|---|---|---|---|---|
| $E$ (MeV) | −94.3 | −81.3 | −80.2 | −78.3 | −76.9 |
| $SO_{1by}$ | 0.83 | 0.43 | 0.41 | 0.20 | 0.24 |
| Proton radius | 2.25 | 2.39 | 2.49 | 2.57 | 2.44 |
| Matter radius | 2.37 | 2.90 | 2.70 | 2.78 | 2.92 |
| $P_v$ | −0.94 | −0.34 | −0.76 | 0.46 | −0.19 |

Here, $\vec{L}_i$ and $\vec{S}$ represent one-body angular momentum and spin operators for the protons. The actual spin-orbit interaction in the Hamiltonian is two-body, but to see the amount of $\alpha$ breaking in the wave function, we introduce this one-body operator. The value is zero for the $3\alpha + n$ model space, because two protons form $S = 0$ in each $\alpha$ cluster. However when one of the $\alpha$ clusters is broken, the value becomes finite. The value is 1 when the wave functions of two protons in one of the $\alpha$ clusters is changed to a $jj$-coupling wave function of $p3/2$, and the value becomes −2 when they occupy the $jj$-coupling wave function of $p1/2$. Therefore, the one-body $ls$ operator for the protons can be a measure of the $\alpha$-breaking effect. The results for the $1/2^-$ states of $^{13}$C are summarized in Table I. The ground $1/2^-$ state calculated at −94.3 MeV has the value of 0.83, which shows that one of the $\alpha$ clusters is completely changed into a $jj$-coupling-like wave function. However, the value decreases with increasing excitation energy. Therefore, we confirm the persistence of the $\alpha$-cluster structure in the excited states.

The proton and matter rms radii for the $1/2^-$ states calculated within the bound state approximation are also shown in Table I. The ground $1/2^-$ state has a small radii of 2.25 fm (proton) and 2.37 fm (matter), and these results are consistent with our previous statement that the shell-model-like components are dominant in this state. The matter radii for the $1/2^-$ states have a tendency to increase with the increase of the excitation energy. The matter radius for the $1/2^-$ state at −81.3 MeV ($E_x = 13.0$ MeV) is especially large, which corresponds to the dilute distribution of valence neutron as shown in Fig. 2(b), which we mention later. The fourth $1/2^-$ state calculated at −78.3 MeV ($E_x = 16.0$ MeV) has a large proton radius (2.57 fm) and a small $\alpha$-breaking component ($\langle SO_{1by} \rangle = 0.20$), which indicates the presence of an $\alpha$-cluster structure in this state.

Next, we analyze the single-particle parity of one valence neutron moving around the $^{12}$C core, which is shown as $P_v$ in Table I. The single-particle parity of the valence neutron can be calculated by introducing the following operator [30]:

$$P_v = \sum_{i=\text{neutrons}} \hat{P}_i - \sum_{i=\text{protons}} \hat{P}_i. \quad (7)$$

Here, $\hat{P}_i$ is the parity inversion operator of the $i$-th nucleon, and the eigenvalue is $1\,(−1)$ for the nucleon in the positive-parity (negative-parity) orbit. By subtracting the proton part from the neutron part, the contribution coming from the $^{12}$C core disappears and we can extract the information of the valence neutron. The ground state has the expectation value of −0.94, which is close to −1 because the valence neutron mainly occupies the $p$ orbital around the $^{12}$C core. The valence neutron in the third $1/2^-$ state also has a value close to $−1\,(−0.76)$; however, the second and fifth $1/2^-$ states have the values of −0.34 and −0.19, respectively. Here the valence neutron has both the positive- and negative-parity components. On the contrary, the fourth $1/2^-$ state has a positive value (0.46), thus the negative parity is created by the $^{12}$C core.

The intrinsic density of each $1/2^-$ state is shown in Fig. 2. In our calculation, we have superposed many Slater determinants, and the coefficients for the linear combination are obtained after the angular momentum and parity projections; however, the intrinsic density can be extracted in a way shown in Ref. [31]. Each bases state is rotated to be the eigen state of the $Q$ operator, and the coefficients for the linear combination of the basis states are modified by multiplying Wigner's $D$ function. Here, the blue contour lines show the intrinsic density of the protons, which is proportional to the density distribution of the $^{12}$C core part, and by subtracting the proton density from
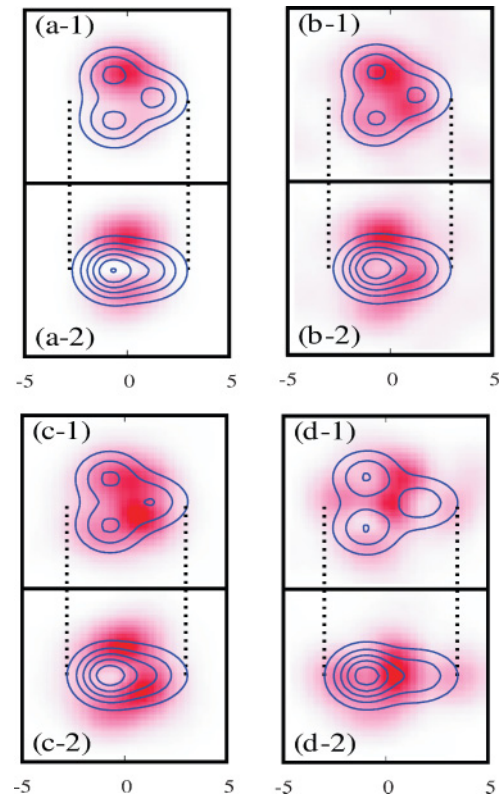


FIG. 2. (Color online) Density distribution of each $1/2^-$ states of $^{13}$C [$1/2_1^-$ (a), $1/2_2^-$ (b), $1/2_3^-$ (c), and $1/2_4^-$ (d)]. The blue dotted curves show the density of the proton part (proportional to the distribution of the $^{12}$C core), and the density distribution of the valence neutron is shown by the red dots. The distributions on the $xy(xz)$ plane are shown with the label of "-1" ("-2").

the neutron density we obtain the density distribution of the valence neutron, which is shown by the red dots. The blue lines show that the clustering of $3\alpha$ develops with increasing excitation energy, which is consistent with our results in Table I. The valence neutron (red dots) has a specific distribution in each state. In the ground state, the valence neutron is concentrated around the $^{12}$C core [Fig. 2(a-1)] and it has a clear node perpendicular to the $3\alpha$ plane [Fig. 2(a-2)]. In the second $1/2^-$ state, the valence neutron has a dilute distribution around the $^{12}$C core [Fig. 2(b-1)], and the node perpendicular to the $3\alpha$ plane is vague compared with the ground state [Fig. 2(b-2)]. In the fourth $1/2^-$ state [Fig. 2(d)], the density of the valence neutron is localized around the center of three $\alpha$ clusters without a node, which is consistent with the calculated positive value of the single-particle parity shown in Table I.

Next, we check whether the calculated $1/2^-$ states above the particle threshold really correspond to the sharp resonance states that can be observed by experiments or not. By using the idea of analytical continuation in the coupling constant (ACCC) [32–34], we can investigate the behavior of the solution with additional potential $V_{1by}$ with the coupling constant $\lambda$, by which nucleons are more attracted into the inner region. When the energy of some specific state is exceptionally insensitive to the $\lambda$ value, we consider the corresponding state continuum state or broad resonance state. In the present case, the spatial extension of each $\alpha$ cluster is compact compared with the one valence neutron; this is most specific in the second $1/2^-$ state as shown in Fig. 2 and Table I. Therefore, we focus on the valence neutron and apply this method, and the additional potential is set to have the following form:

$$V_{1by} = \lambda \left\{ \sum_{i=\text{neutrons}} G(i) - \sum_{i=\text{protons}} G(i) \right\}, \qquad (8)$$

where $G(i) = V_g \exp\{-\nu_g (r_i - r_{\text{c.m.}})^2\}$ is the one-body Gaussian potential with $V_g$ (depth) $= -51$ MeV and $\nu_g$ (range parameter) $= 0.1$ fm$^{-2}$. The contribution of the potential to the proton part is subtracted from the neutron part; thus the effect for the $^{12}$C core vanishes and the additional potential acts only for one valence neutron around $^{12}$C. The strength of this additional one-body potential is controlled by the coupling constant $\lambda$.

In Fig. 3, the energies of $1/2^-$ states are shown as a function of the coupling constant $\lambda$. We can see rapid decrease of energy in most of the states with increasing $\lambda$, as seen for the ground, third, and fourth states at $\lambda = 0$; this is the typical behavior for the bound and sharp resonance states. However, there are two states that are less sensitive to the $\lambda$ value. The second $1/2^-$ state at $-81.3$ MeV at $\lambda = 0$ stays almost constant with increasing $\lambda$ value. Although the level experiences the crossings with other states and it corresponds to the seventh $1/2^-$ state at $-82.7$ MeV at $\lambda = 1$, the components of the wave function do not change from $\Lambda = 0$. Such behavior is for the broad resonance or continuum state. Similar thing happens for the fifth $1/2^-$ state at $-76.9$ MeV at $\lambda = 0$. With increasing $\lambda$ value, the state experiences the level crossings, and eventually it becomes the eighth $1/2^-$ state at $\lambda = 1$,
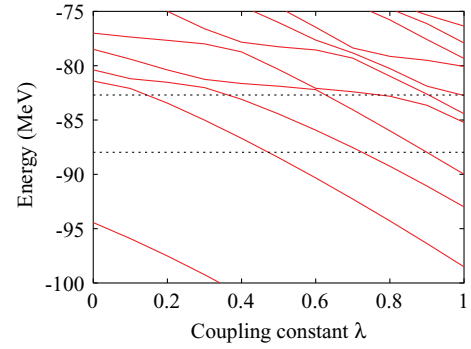


FIG. 3. (Color online) Energies of the $1/2^-$ states of $^{13}$C as a function of coupling constant ($\lambda$) of one-body Gaussian potential [Eq. (8)]. The dashed lines at $-88.0$ and $-82.7$ MeV show the $^{12}$C $+ n$ and $\alpha$-$\alpha$-$\alpha$-$n$ threshold energies, respectively.

however the energy and the property of the wave function stay constant. This state is also considered as a broad resonance state. By performing ACCC with respect to the $^{12}$C $+ n$ threshold energy, the widths for the third and fourth $1/2^-$ states are calculated as 0.5 and 0.2 MeV, respectively. However, we cannot obtained well-converged widths for the second and fifth $1/2^-$ states, which are considered to be broad resonance states as mentioned before. One reason is that our framework is based on the strong coupling picture, and in each basis state only the total system of $^{13}$C is projected to the eigen state of the angular momentum, but the $^{12}$C core part is not. Of course the GCM effect (superposition of many different Slater determinants) helps to restore the rotational symmetry of the $^{12}$C core part; however, the precision for the reproduction of the threshold energy may not be enough for the broad resonance states.

In Fig. 4, the obtained $1/2^-$ states of both cases of $M$ (Majorana exchange parameter of $V2$) $= 0.6$ and $M = 0.61$ are shown together with the experimental results (shown as exp.). Here, the states considered to have large decay width as a result of ACCC analysis are shown by a dotted line (the second and fifth $1/2^-$ states).
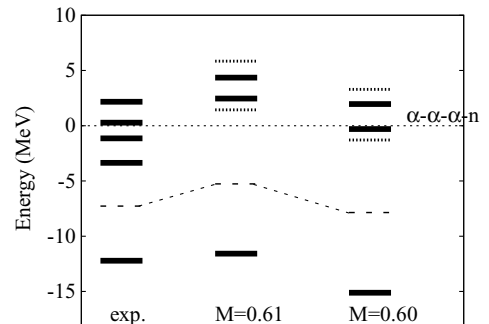


FIG. 4. The energy spectra for the $1/2^-$ states of $^{13}$C measured from the $\alpha$-$\alpha$-$\alpha$-$n$ threshold energy. Both results for $M = 0.61$ and $M = 0.60$ are presented together with the experimental results (shown as exp.). Here, states considered to have a large decay width as a result of ACCC analysis are shown by dotted lines. The dashed lines show the $^{12}$C $+ n$ threshold energy.

## IV. DISCUSSION FOR THE $E0$ TRANSITION

In this section, we discuss the relation between the clustering of each state and the $E0$ transition probabilities. The isoscalar $E0$ transition probability between $i$-th and $j$-th states is given by

$$B(E0, i \rightarrow j) = \left| \langle i | \sum_k r_k^2 | j \rangle \right|^2 , \tag{9}$$

where the summation over $k$ is for all the protons and neutrons. We compare the $B(E0)$ values of $^{12}$C and $^{13}$C and show how the effects of large clustering and $\alpha$ breaking influence the transition probabilities.

We start the discussion with $^{12}$C by introducing a simple model. First, the model space is restricted to three $\alpha$ clusters. The relative distance between two of the $\alpha$ clusters is set to 3 fm. The relative distance between this $^8$Be $(2\alpha)$ and the remaining $\alpha$ (localized perpendicular to $^8$Be) is taken from 2 to 6 fm, which is called $D$. Here, the basis state with $D = 2$ fm is considered to represent the ground state component, and we diagonalize the Hamiltonian consisting of the basis state and another basis state with a different $D$ value. The $E0$ transition probability between these two states after diagonalizing the $2 \times 2$ Hamiltonian is shown as a function of $D$ in Fig. 5 (solid line). The B$(E0)$ value increases with an increase of $D$, and after becoming maximum around $D = 5$ fm, the value decreases rapidly. This maximum value of $\sim$350 fm$^4$ is much larger than the observed $B(E0, 0_1^+ \rightarrow 0_2^+)$ value of 120.1 fm$^4$ [35]. However, the second $0^+$ of $^{12}$C has a dilute distribution of three $\alpha$ clusters, thus the real $B(E0)$ value is integrated over the wide range of the $D$ values. The contribution from the basis states with $D$ larger than 5 fm decreases the expectation value of the $B(E0)$ value. Although the observed $B(E0, 0_1^+ \rightarrow 0_2^+)$ value of $^{12}$C is large and this is the signature of the cluster structure of the second $0^+$ state, if the second $0^+$ state has a definite configuration with $D = 5$ fm, the value must be even larger. When the final state has a very extended density distribution, no spatial overlap with the initial state exists, and the $B(E0)$ value becomes small, so that the experimental $B(E0)$ value of $^{12}$C contains a contribution of such components.

Second, we discuss the contribution of the $\alpha$-breaking effect to the $B(E0)$ value. We prepare the basis states with
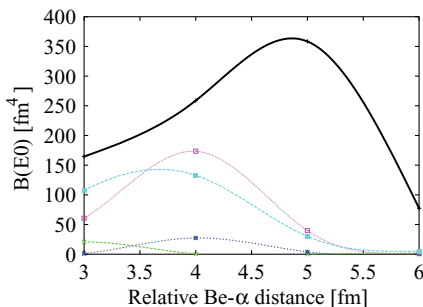
FIG. 5. (Color online) $B(E0)$ value from the ground state as a function of relative $^8$Be-$\alpha$ distance ($D$ in the text). The solid curve shows the results for the second $0^+$ state of $^{12}$C. The dotted curves show the results for the $1/2^-$ states of $^{13}$C.
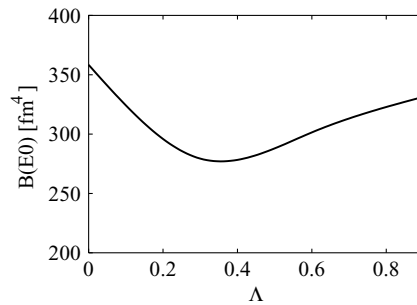
FIG. 6. The $\Lambda$ dependence of the $B(E0, 0_1^+ \rightarrow 0_2^+)$ value of $^{12}$C. See the text for details.

$D = 2$ fm and $D = 5$ fm. After diagonalizing the Hamiltonian, we calculate the $B(E0)$ value between the two obtained states, with the result corresponding to $D = 5$ fm in Fig. 5. Here, we calculate the change of the $B(E0)$ value when one of the $\alpha$ clusters in the $D = 2$ (fm) basis state is broken due to the spin-orbit interaction. The breaking effect of one of the $\alpha$ clusters is expressed by introducing $\Lambda$ as in the previous section. Figure 6 shows the $\Lambda$ dependence of the $B(E0)$ value, and we can see the decrease of the value when one $\alpha$ cluster is broken into four independent particles. The curve indicates that the mixing of the shell-model-like configurations in the ground state of $^{12}$C contributes to the decrease of the $B(E0)$ value to about 25 % around $\Lambda = 0.4$, which is the optimal $\Lambda$ value for the ground state of $^{12}$C. This is another reason why the observed $B(E0, 0_1^+ \rightarrow 0_2^+)$ value of $^{12}$C is much smaller than the maximum value of Fig. 5.

Finally, we discuss the case of $^{13}$C. Here, the $^{12}$C core is also described by the three $\alpha$ clusters, and we prepare the basis states with $D = 2$ fm and different $D$ values. Moreover, we superpose the basis states, which are generated by using a random number for the Gaussian center parameter of the valence neutron. The selection of the basis state is performed in the same way as described in Sec. III. In Fig. 5, the dotted lines show the $B(E0)$ values of $^{13}$C between the ground $1/2^-$ state and the excited $1/2^-$ states as functions of $D$. The values are strongly dependent on the neutron orbit of the final state, and generally, they are much smaller than those of the $^{12}$C case.

TABLE II. Relation between $E0$ transition strength and "disparity" ($|P_v^i - P_v^f|$) of the valence neutron (in parentheses) for various $1/2^-$ states of $^{13}$C. Note that the model space of this table is the one used in Sec. III.

| States | $1/2_1^-$ | $1/2_2^-$ | $1/2_3^-$ | $1/2_4^-$ | $1/2_5^-$ |
|---|---|---|---|---|---|
| Single-particle parity ($P_v$) | $-0.94$ | $-0.34$ | $-0.76$ | $0.46$ | $-0.19$ |
| $1/2_1^-$ | | 65.6 | 121.6 | 2.8 | 0.0 |
| | | (0.60) | (0.18) | (1.4) | (0.75) |
| $1/2_2^-$ | | | 61.0 | 20.0 | 24.7 |
| | | | (0.42) | (0.80) | (0.15) |
| $1/2_3^-$ | | | | 0.2 | 29.3 |
| | | | | (1.22) | (0.57) |

Here, we show how the wave function of one valence neutron causes the suppression of the $B(E0)$ value, which is remarkable at some specific condition. The matrix element of the $E0$ transition in $^{13}$C between the initial ($i$) and the final ($f$) states ($M(i \rightarrow f)$) can be roughly expressed by the two terms

$$M(i \rightarrow f) = \langle \psi_{vn}^i | r^2 | \psi_{vn}^f \rangle \times \langle \Psi_{3\alpha}^i | \Psi_{3\alpha}^f \rangle$$
$$+ \langle \psi_{vn}^i | \psi_{vn}^f \rangle \times \langle \Psi_{3\alpha}^i | \sum_k r_k^2 | \Psi_{3\alpha}^f \rangle, \quad (10)$$

where $\psi_{vn}$ and $\Psi_{3\alpha}$ denote the wave functions for the valence neutron and the $3\alpha$ core, respectively. In this case, the second term is more important, because this is the coherent sum of 12 nucleons in the $^{12}$C core. Furthermore, this term is nothing but the value for the $^{12}$C core part with the factor of $\langle \psi_{vn}^i | \psi_{vn}^f \rangle$. Therefore, in the case of the $E0$ transition of $^{13}$C, an additional factor, which is the overlap of the wave function of the valence neutron between the initial and final states, is multiplied to the transition probability of $^{12}$C. Our discussion for the relation between the $B(E0)$ value and the wave function suggests that the "disparity" of the orbit of the valence neutron between the initial and final states affects the $B(E0)$ value sensitively. To see this effect, we define the disparity of the wave function of the valence neutron in the initial and final states, which is the difference of the single-particle parity ($P_v$)

of the initial ($i$) and final ($f$) states, $|P_v^i - P_v^f|$. Using the model space of Sec. III, we can discuss the relation between the disparity and the $B(E0)$ values. Table II indicates that the $B(E0)$ value becomes small when the disparity is large, and this is prominent in $B(E0, 1/2_1^- \rightarrow 1/2_4^-)$. This is the reason why the state calculated at $E_x = 16$ MeV, which has a large clustering feature, has a small $E0$ transition probability from the ground state.

## V. CONCLUSION

We have studied the structure of $^{13}$C with a microscopic model. In addition to the cluster structure, the $\alpha$-breaking configurations using SMSO are included. The energy spectra of the $1/2^-$ states are obtained reasonably compared with the experimental ones. Although the $\alpha$-breaking effect is found to be prominent in the ground state, the $\alpha$-cluster structure becomes important with increasing excitation energy. We discussed the relation between the clustering of each state and the $E0$ transition probabilities. In $^{13}$C, the overlap of the wave function of the valence neutron between the initial and final states is multiplied to the transition probability of $^{12}$C. Therefore, the "disparity" in the orbit of the valence neutron between the initial and final states affects the $B(E0)$ value sensitively.

[1] D. M. Brink, in *Proceedings of the International School of Physics "Enrico Fermi" Course XXXVI*, edited by C. Bloch (Academic, New York, 1966), p. 247.

[2] Y. Fujiwara, H. Horiuchi, K. Ikeda, M. Kamimura, K. Katō, Y. Suzuki, and E. Uegaki, Prog. Theor. Phys. Suppl. **68**, 60 (1980).

[3] M. Freer *et al.*, Phys. Rev. Lett. **82**, 1383 (1999); M. Freer *et al.*, Phys. Rev. C **63**, 034301 (2001).

[4] W. von Oertzen, Z. Phys. A **354**, 37 (1996); **357**, 355 (1997).

[5] Y. Kanada-En'yo, H. Horiuchi, and A. Dote, Phys. Rev. C **60**, 064304 (1999).

[6] Y. Ogawa, K. Arai, Y. Suzuki, and K. Varga, Nucl. Phys. **A673**, 122 (2000).

[7] M. Ito, N. Itagaki, H. Sakurai, and K. Ikeda, Phys. Rev. Lett. **100**, 182502 (2008); M. Ito and N. Itagaki, Phys. Rev. C **78**, 011602(R) (2008).

[8] N. Itagaki and S. Okabe, Phys. Rev. C **61**, 044306 (2000); N. Itagaki, S. Hirose, T. Otsuka, S. Okabe, and K. Ikeda, Phys. Rev. C **65**, 044302 (2002); N. Itagaki, S. Okabe, and K. Ikeda, Phys. Rev. C **62**, 034301 (2000).

[9] P. Descouvemont, Nucl. Phys. **A699**, 463 (2002).

[10] K. Arai, Phys. Rev. C **69**, 014309 (2004).

[11] A. Tohsaki, H. Horiuchi, P. Schuck, and G. Röpke, Phys. Rev. Lett. **87**, 192501 (2001).

[12] P. Schuck, Y. Funaki, H. Horiuchi, G. Röpke, A. Tohsaki, and T. Yamada, Nucl. Phys. **A738**, 94 (2004).

[13] N. Itagaki, T. Otsuka, K. Ikeda, and S. Okabe, Phys. Rev. Lett. **92**, 142501 (2004).

[14] R. Bijker and F. Iachello, Phys. Rev. C **61**, 067305 (2000).

[15] W. von Oertzen *et al.*, Eur. Phys. J. A **21**, 193 (2004).

[16] Y. Sasamoto *et al.*, Mod. Phys. Lett. A **21**, 2393 (2006).

[17] M. Milin *et al.*, Eur. Phys. J. A **14**, 295 (2002).

[18] D. L. Price *et al.*, Nucl. Phys. **A765**, 263 (2006).

[19] P. J. Haigh *et al.*, Phys. Rev. C **78**, 014319 (2008).

[20] Taiichi Yamada, Hisashi Horiuchi, and Peter Schuck, Mod. Phys. Lett. A **21**, 2373 (2006).

[21] N. Itagaki, H. Masui, M. Ito, and S. Aoyama, Phys. Rev. C **71**, 064307 (2005).

[22] H. Masui and N. Itagaki, Phys. Rev. C **75**, 054309 (2007).

[23] N. Itagaki, S. Aoyama, S. Okabe, and K. Ikeda, Phys. Rev. C **70**, 054307 (2004).

[24] A. B. Volkov, Nucl. Phys. **74**, 33 (1965).

[25] R. Tamagaki, Prog. Theor. Phys. **39**, 91 (1968).

[26] S. Okabe and Y. Abe, Prog. Theor. Phys. **61**, 1049 (1979).

[27] G. Thiamova *et al.*, Eur. Phys. J. A **22**, 461 (2004).

[28] T. Otsuka, T. Matsuo, and D. Abe, Phys. Rev. Lett. **97**, 162501 (2006).

[29] K. Varga, Y. Suzuki, and Y. Ohbayasi, Phys. Rev. C **50**, 189 (1994).

[30] N. Itagaki, W. von Oertzen, and S. Okabe, Phys. Rev. C **74**, 067304 (2006).

[31] S. C. Pieper and R. B. Wiringa, Annu. Rev. Nucl. Part. Sci. **51**, 53 (2001).

[32] V. I. Kukulin, V. M. Krasnopol'sky, and J. Horacek, *Theory of Resonances: Principles and Applications* (The Kluwer Academic, Dordrecht, Netherlands, 1989), p. 219.

[33] N. Tanaka, Y. Suzuki, K. Varga, and R. G. Lovas, Phys. Rev. C **59**, 1391 (1999).

[34] Y. Funaki, H. Horiuchi, and A. Tohsaki, Prog. Theor. Phys. **115**, 115 (2006).

[35] F. Ajzenberg-Selove, Nucl. Phys. **A506**, 1 (1990).